Evaluating EDGARv4.tox2 speciated mercury emissions ex-post scenarios and their impacts on modelled global and regional wet deposition patterns

Atmospheric Environment 184 (2018) 56–68

Contents lists available at ScienceDirect

Atmospheric Environment

journal homepage: www.elsevier.com/locate/atmosenv

Evaluating EDGARv4.tox2 speciated mercury emissions ex-post scenarios and their impacts on modelled global and regional wet deposition patterns

Marilena Muntean[a,*], Greet Janssens-Maenhout[a], Shaojie Song[b,1], Amanda Giang[b], Noelle E. Selin[b], Hui Zhong[c], Yu Zhao[c], Jos G.J. Olivier[d], Diego Guizzardi[e], Monica Crippa[a], Edwin Schaaf[a], Frank Dentener[f]

[a] European Commission, Joint Research Centre (JRC), Directorate for Energy, Transport and Climate, Air and Climate Unit, Via E. Fermi 2749, I-21027, Ispra, VA, Italy
[b] Massachusetts Institute of Technology, Cambridge, MA, United States
[c] State Key Laboratory of Pollution Control & Resource Reuse and School of the Environment, Nanjing University, 163 Xianlin Ave., Nanjing, Jiangsu, 210023, China
[d] PBL Netherlands Environment Assessment Agency, Bilthoven, The Netherlands
[e] Didesk Informatica, Verbania, VB, Italy
[f] European Commission, Joint Research Centre (JRC), Directorate for Sustainable Resources, Food Security Unit, Via E. Fermi 2749, I-21027, Ispra, VA, Italy

ARTICLE INFO

Keywords:
Mercury
Emissions inventory
Speciation scenarios
Global and nested simulations
Wet deposition

ABSTRACT

Speciated mercury gridded emissions inventories together with chemical transport models and concentration measurements are essential when investigating both the effectiveness of mitigation measures and the mercury cycle in the environment. Since different mercury species have contrasting behaviour in the atmosphere, their proportion in anthropogenic emissions could determine the spatial impacts. In this study, the time series from 1970 to 2012 of the EDGARv4.tox2 global mercury emissions inventory are described; the total global mercury emission in 2010 is 1772 tonnes. Global grid-maps with geospatial distribution of mercury emissions at a $0.1^{\circ} \times 0.1^{\circ}$ resolution are provided for each year. Compared to the previous tox1 version, tox2 provides updates for more recent years and improved emissions in particular for agricultural waste burning, power generation and artisanal and small-scale gold mining (ASGM) sectors. We have also developed three retrospective emissions scenarios based on different hypotheses related to the proportion of mercury species in the total mercury emissions for each activity sector; improvements in emissions speciation are seen when using information primarily from field measurements. We evaluated them using the GEOS-Chem 3-D mercury model in order to explore the influence of speciation shifts, to reactive mercury forms in particular, on regional wet deposition patterns. The reference scenario S1 (EDGARv4.tox2_S1) uses speciation factors from the Arctic Monitoring and Assessment Programme (AMAP); scenario S2 ("EPA_power") uses factors from EPA's Information Collection Request (ICR); and scenario S3 ("Asia_filedM") factors from recent scientific publications. In the reference scenario, the sum of reactive mercury emissions (Hg-P and Hg^{2+}) accounted for 25.3% of the total global emissions; the regions/countries that have shares of reactive mercury emissions higher than 6% in total global reactive mercury are China+ (30.9%), India+ (12.5%) and the United States (9.9%). In 2010, the variations of reactive mercury emissions amongst the different scenarios are in the range of −19.3 t/yr (China+) to 4.4 t/yr (OECD_Europe). However, at the sector level, the variation could be different, e.g., for the iron and steel industry in China reaches 15.4 t/yr. Model evaluation at the global level shows a variation of approximately ± 10% in wet deposition for the three emissions scenarios. An evaluation of the impact of mercury speciation within nested grid sensitivity simulations is performed for the United States and modelled wet deposition fluxes are compared with measurements. These studies show that using the S2 and S3 emissions of reactive mercury, can improve wet deposition estimates near sources.

1. Introduction

Mitigation of mercury is addressed internationally by actions stipulated in the Long-range Transboundary Air Pollution Convention, Protocol on Heavy Metals (UNECE, 1998) of the United Nations Economic Commission for Europe (UNECE), complemented and extended

* Corresponding author.
E-mail address: marilena.muntean@ec.europa.eu (M. Muntean).
[1] Now at School of Engineering and Applied Sciences, Harvard University, Cambridge, MA, United States.

https://doi.org/10.1016/j.atmosenv.2018.04.017
Received 30 October 2017; Received in revised form 6 April 2018; Accepted 9 April 2018
Available online 10 April 2018

to the global level by the provisions of the Minamata Convention (UNEP, 2013b) of the United Nations Environmental Programme (UNEP). This framework streamlines the efforts towards reducing the harmful impacts of mercury and its compounds on human health and the environment at global, regional and local scales.

Mercury impacts at different scales are associated with the emission of mercury species into the atmosphere (Liu et al., 2010a; Schleicher et al., 2016). Evidence from transport modelling studies shows a direct relationship between emissions and concentrations of reactive mercury at measurement stations (Gratz et al., 2013a, 2013b) and de Foy et al. (2014) highlight the importance of improving emission inventories, in particular for reactive mercury species. Both emissions inventories and in-situ atmospheric measurements distinguish between gaseous elemental mercury (Hg^0) and reactive mercury (Hg-P and Hg^{2+}). The lifetime of each mercury species emitted into atmosphere depends on its individual reactivity. The less reactive Hg^0 has an atmospheric lifetime of several months to a year, whereas particle-bound mercury (Hg-P) has 1–2 weeks lifetime and gaseous oxidised mercury (Hg^{2+}) has a lifetime that ranges from hours to days, due to its high solubility. As a consequence, when emitted into the atmosphere Hg^{2+} deposits relatively close to the sources, affecting the nearby environment; the local oxidation of Hg^0, which is dependent on meteorological conditions, can also add Hg^{2+} to the existing levels (Sigler et al., 2009). The relative abundance of the different mercury species in the atmosphere, besides meteorological conditions and land surface exchange parameters, are key factors in determining the level of deposition (Lyman et al., 2007), which further contributes to the formation of organic mercury in the environment. Mercury deposition occurs during precipitation events (wet) and in the absence of precipitation (dry); wet deposition processes primarily scavenge the reactive forms of mercury from the atmosphere i.e., Hg^{2+} and Hg-P (Zhang et al., 2012a), while Hg^0 is unaffected.

Measurements of anthropogenic mercury emissions from different sources such as power plants, incinerators, cement and iron and steel factories, nonferrous metal manufacturing and mobile sources show that mercury speciation, i.e., Hg^0 and Hg-P + Hg^{2+} is sector specific (Kim et al., 2010). For some of these sectors, detailed mercury speciation profiles are available. For instance, studies have measured emissions speciation from coal-fired power plants, a relevant emissions source of reactive mercury, taking into account factors such as air pollution control devices, temperature, additives and coal type, composition and size (Gharebaghi et al., 2011; Jang et al., 2014; Jongwana and Crouch, 2012; Liu et al., 2010b; Ochoa-González et al., 2011; Omine et al., 2012; Rallo et al., 2012; Schofield, 2012; Tang et al., 2016; Wu et al., 2010; Yu et al., 2015; Zhang et al., 2013). Similar measurements have been conducted for industrial cement production facilities, iron and steel plants (Wang et al., 2014), and non-ferrous metal smelters (Ye et al., 2015). Together, these studies suggest that the main factors determining sectorial variations in speciation are input fuel or ore, operational processes, and control technologies.

Focusing on the more reactive mercury forms, i.e., Hg^{2+} and Hg-P, in this study, we explore how various scenarios of mercury species emissions could reproduce regional scale features of mercury atmospheric observations and wet deposition in particular, by using a global gridded mercury emissions inventory as input for a chemical transport model.

The Emission Database for Global Atmospheric Research version tox2 (hereafter EDGARv4.tox2) contains mercury emissions time series from 1970 to 2012 for all of countries in the world. EDGARv4.tox2 provides total mercury (Hg) as well as speciated mercury emissions: gaseous elemental mercury (GEM) (Hg^0), gaseous oxidized mercury (GOM) (Hg^{2+}) and particle-bound mercury (PBM) (Hg-P). This global mercury emissions inventory, which includes emissions from all key mercury emitting sources, is an updated version of EDGARv4.tox1 (Muntean et al., 2014). Total mercury emissions (Hg) are calculated based on activity data from international statistics and emission factors from several widely used official datasets. Emissions of the mercury species Hg^0, Hg^{2+} and Hg-P are derived by applying different speciation factors.

Three different mercury species retrospective (ex-post) emissions scenarios were developed by using information on speciation factors from AMAP/UNEP (2008), EPA's ICR (Bullock and Johnson, 2011) and recent scientific literature (AMAP/UNEP, 2008; Chen et al., 2013; Friedli et al., 2001; Friedli et al., 2003a; Friedli et al., 2003b; Giang et al., 2015; Park et al., 2008; UNEP, 2014; Wu et al., 2012; Zhang et al., 2015). The reference scenario (S1) includes Hg emissions from which emissions of Hg^0, Hg^{2+} and Hg-P were estimated by applying AMAP speciation factors for all sectors. In scenario 2 (S2) the emissions are the same as in S1 apart from the power generation sector where the speciation profiles of the US EPA's ICR database are used. For scenario 3 (S3), the proportion of each mercury species in total mercury emissions was estimated from information about sector-specific speciation profiles in recent publications, focusing on measurements from emerging economies (references above). As a result, the three scenarios, which are described in section 2, capture both sectorial and geographical variations in speciation, and can be used to evaluate potential implications for wet deposition patterns.

We used the GEOS-Chem chemical transport model to evaluate the three mercury species emission scenarios. The results are presented and discussed for both global and nested-grid simulations in section 3.

2. Methodology

In developing this new version of the EDGAR global anthropogenic mercury emissions inventory EDGARv4.tox2, we focused not only on emissions estimation for the most recent years but also on revising and updating the historical emissions of key sources characterised by large uncertainties, based on the latest available information. Given that mercury species have impacts at both global and local scales, we included a new mercury emissions source, that of transportation, which could produce more local effects. We also developed three speciated ex-post emissions scenarios and used them as input in a chemical transport model in order to better understand the complex processes undergone by speciated mercury within the atmosphere.

2.1. Methodology for updating the EDGAR global gridded anthropogenic mercury emissions

The activity data in EDGARv4.tox1 has been updated for both large scale and artisanal small-scale gold mining, chlor-alkali production using mercury cell technology and mercury mining; for the rest of the sectors the activity data are those of EDGARv4.3.2 (Janssens-Maenhout et al., 2017). Together, these give the new version EDGARv4.tox2 containing mercury emission time series from 1970 to 2012 for all of the countries in the world. It includes emissions of total mercury (Hg) and Hg^0, Hg^{2+} and Hg-P mercury species. The EDGAR methodology to estimate global mercury emissions is described in Muntean et al. (2014). It relies on activity data, emission factors and control measures information from international data sources for key mercury emissions sources, i.e., agricultural waste burning, chlor-alkali, power generation, combustion in industry and residential, cement and glass production, non-ferrous and iron & steel industries, waste incineration and transport.

The activity data have been updated by using statistics from International Energy Agency (IEA, 2014) for fuel consumption, United States Geological Survey (USGS, 2015) for metal and cement production, Food and Agriculture Organization of United Nations (FAO, 2015) for agricultural waste burning, information from national reporting to United Nations Framework Convention on Climate Change (UNFCCC, 2015) for solid waste incineration and reports of specialized international institutions for the chlor-alkali and artisanal and small-scale gold mining (ASGM) sectors.

The updates to activity data (AD), emission factors (EFs) and control measures, namely: electrostatic precipitator (ESP); fabric filter (FF); selective catalytic (SCR) and non-catalytic (SNCR) reduction; wet and dry flue-gas desulphurisation (FGD), applied to different sectors resulted in substantial differences between the two EDGARv4 versions of the global mercury emissions inventories. The largest differences in mercury emissions in EDGARv4.tox2 compared to EDGARv4.tox1 are in the agricultural waste burning, power generation and ASGM sectors. The overall difference between the emissions inventories is an increase of 350 tonnes in 2008, the final year of the tox1 dataset, which represents an increase of 27.2% in mercury emissions in tox2 compared to tox1.

The parameters used as input by EDGAR to estimate mercury emissions are primarily those described by Muntean et al. (2014) with some updates as presented in this section. An improved EF, used in emissions calculation for agricultural waste burning, from the "air pollutant emissions inventory guidebook" of the European Monitoring and Evaluation Programme (EMEP) and European Environment Agency (EEA) (EMEP/EEA, 2013), which is 17.5 times higher than the EF used in EDGARv4.tox1 for agricultural waste burning resulted in higher mercury emissions from 1970 to 2012 for all countries. Updated activity data for sinter production in the iron & steel industry and new activity data for the ASGM sector from the Artisanal Gold Council (AGC, 2010b) led to an improved emissions estimation for these sectors, resulting in global increases of 25.6% and 56.8%, respectively, in 2008. For the power generation sector, AD from IEA (2014) release and updated end-of-pipe (EoP) allocation applied to power plants in China led to an increase of mercury emissions in tox2 e.g., by 5.5% in 2008. For China, detailed information from individual power plants was used to update the EoP systems in EDGARv4.tox2 from 2005 onwards, based an updated power plant database from Zhao et al. (2008). As presented in Fig. Si1 of the Supporting Information (Si), implementation of the EoP in China is characterised by an increased utilisation of advanced control systems in recent years. The main players were ESP, which decreased its share in total mitigation technology in China from 73% in 2005 to 11% in 2012, and ESP + wetFGD, which increased from 9% to 57% in the same period; advanced control systems, i.e., SCR + ESP + wetFGD, were introduced in 2010 and reached 28% in 2012. All these improvements in input data are reflected in the mercury emissions levels.

The clinker content in cement has been updated from 2000 until 2012 with info from CSI (2016) for the majority of the countries in the world and for China with info from Xu et al. (2014). Fig. Si2 provides the variability in clinker content in cement from 2000 until 2012 by region. These parameters are used to calculate country specific EFs for the cement production sector. China, which is the largest cement producer (58% share) in the world, decreased its clinker content in cement by 18% over this period, and India (7% share), which follows China, decreased it by 21%; these decreases result in significant changes in mercury emissions from cement production in these countries.

With a time-step length of five years, Fig. Si3 illustrates these emissions changes giving details on sector contribution for both inventories over the 1970-(2008)2012 period.

A new mercury emissions source, the transportation sector was included in the EDGARv4.tox2 version, enhancing the coverage of emissions sources relevant for urban areas where chemical mixtures affect human exposures. Mercury emissions have been calculated for road transportation, inland waterways and international shipping by multiplying the fuel consumption (IEA, 2014) with emission factors (EMEP/EEA, 2013). The EFs used in this study are 8.7 μg/kg for gasoline and 5.3 μg/kg for diesel in road transportation, and 20 μg/kg for bunker fuel and 30 μg/kg marine diesel oil/gas oil in domestic and international shipping; the EFs in the transport sector are fuel dependent.

2.2. Definition of mercury speciation ex-post emission scenarios (S1, S2, S3)

The EDGARv4.tox2 contains global mercury emissions for each country in the world as Hg and in addition speciated in the mercury species: Hg^0, Hg^{2+} and Hg-P. As described by Muntean et al. (2014), the emissions of mercury species for each sector are calculated by multiplying the total Hg emissions with technology-based and EoP-based speciation factors (%) which are specific to each sector. The type of control device can affect mercury species formation.

We developed the mercury speciation ex-post emission scenarios based on an early version of EDGAR.v4.tox2, named hereafter EDGARv4.tox2_S1 or S1. In S1, the reference scenario, for all the sectors, the speciation factors are the widely used AMAP/UNEP (2008) speciation factors. In S2, the speciation factors for the power generation sector globally are from US EPA's ICR (Bullock and Johnson, 2011) and from AMAP/UNEP (2008) for all other sectors. In S3 we used speciation factors primarily from recently published scientific literature, focusing on measurements from emerging economies in East and South Asia, but applied globally ((AMAP/UNEP, 2008; Chen et al., 2013; Friedli et al., 2001; Friedli et al., 2003a; Friedli et al., 2003b; Giang et al., 2015; Park et al., 2008; UNEP, 2014; Wu et al., 2012; Zhang et al., 2015) see Table Si1 and Table Si2), except for the chlor-alkali, gold and mercury production sector for which mercury species emissions have been derived using speciation factors from (AMAP/UNEP, 2008).

In this study, we moved from a basic sectorial mercury species approach (S1) to a more refined emissions estimation methodology for mercury species based on recent findings (S2 and S3). We performed a comprehensive literature review of scientific papers on mercury speciation factors (%); the shares of Hg^0 and of reactive mercury forms (Hg-P and Hg^{2+}) in Hg used in our approach are those presented in Fig. 1. The choice is based on an examination of large amount of information, including field measurements, related to mercury speciation in power generation, combustion in industry and residential, municipal waste incineration, cement production, zinc, lead and copper smelting, iron and steel production and agricultural waste burning (see Tables Si1 and Si2).

Data sources and details on the proportions of mercury species in Hg emissions of the three ex-post scenarios are provided in Tables Si1 and Si2 of the Si for each sector.

2.3. GEOS-Chem chemical transport model: global and nested simulations of mercury

To understand the potential implications of different speciation factors on atmospheric mercury, we conducted simulations with the GEOS-Chem (version 10-01; www.geos-chem.org) chemical transport model. The global scale and long-term impacts of yearly EDGAR.tox1 mercury emissions were evaluated previously in Muntean et al. (2014); in this paper, simulations focus primarily on illustrating the effects of speciation for the years 2010–2012 (when observational data sets are largest) and a high-resolution regional case study of North America (Zhang et al., 2012b) to better capture the potentially localised impacts of reactive mercury emissions changes.

Driven by assimilated meteorological data from the NASA GMAO Goddard Earth Observing System Model Version 5 (GEOS-5), GEOS-Chem mercury simulations dynamically couple a 3-dimensional atmosphere, a 2-dimensional mixed-layer slab ocean and a 2-dimensional terrestrial reservoir (Holmes et al., 2010; Selin et al., 2008; Soerensen et al., 2010). The model was initialised from 2005 to 2009 and results from 2010 to 2012 were used for analysis. Sub-surface ocean concentrations are held constant based on Soerensen et al. (2010) for the simulation period, while the present-day spatial distribution of soil mercury is generated using the method described by Selin et al. (2008). The simulations are at $2^\circ \times 2.5^\circ$ horizontal resolution (degraded from the native GEOS-5 grid) at the global scale. For North America (140-

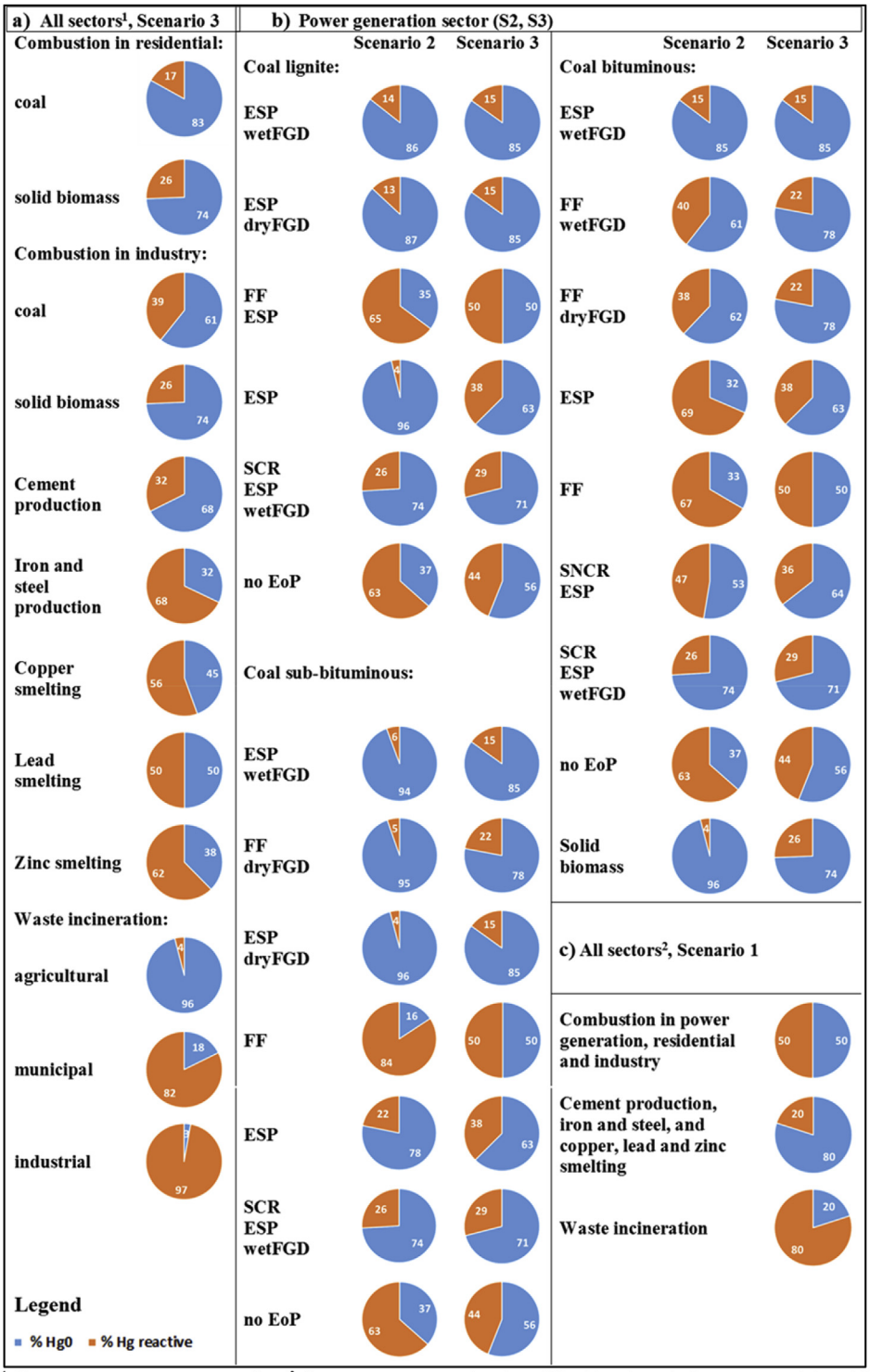

[1]all sectors except power generation; [2]all sectors except: combustion of liquid and gas fuels, mercury mining, ASGM and chlor-alkali industry for which speciation split factors from AMAP/UNEP (2008) were used in all three scenarios.

Fig. 1. Speciation factors used in this study to derive emissions of elemental mercury (Hg^0) and reactive forms of mercury (Hg-P + Hg^{2+}) for S1, S2 and S3: a) all sectors[1] for S3, b) power generation for S1 and S3 and c) all sectors[2] for S1.

40°W, 10–70°N), the model was run in a one-way nested grid formulation with the native GEOS-5 horizontal resolution of 0.5° × 0.667° (Zhang et al., 2012b). The global simulations provide initial and boundary conditions for the nested simulations. For both global and nested simulations, the high-resolution 0.1° × 0.1° EDGARv4.tox2_S1, S2 and S3 speciated mercury emissions are regridded to the simulation grid. Both global and nested simulations have 47 vertical layers in the atmosphere from the surface up to 0.01 hPa.

In addition to anthropogenic emissions from EDGAR, the model simulations include atmospheric mercury fluxes from geogenic activities, biomass burning, soil/vegetation, and ocean (Song et al., 2015). Three mercury tracers (representing Hg^0, Hg^{2+}, and Hg-P) are simulated in the atmosphere in GEOS-Chem.

Atmospheric mercury chemistry follows (Holmes et al., 2010) with

atomic bromine as the predominant oxidant of Hg^0. Atmospheric reduction of oxidised Hg is not included in these simulations as its atmospheric relevance is unknown and an accurate determination of potential chemical pathways is lacking (Subir et al., 2012). In-plume reduction of oxidised Hg emitted from coal-fired power plants is not considered (Zhang et al., 2012b). In the atmosphere both emitted and chemically-formed reactive mercury are assumed to be in equilibrium between the gas phase (Hg^{2+}) and particle phase (Hg-P) at all times (Amos et al., 2012). The wet deposition scheme, which removes reactive mercury from the atmosphere, is described fully in Shah and Jaeglé (2017).

3. Results

3.1. Mercury emissions trends over four decades and emissions distribution in EDGARv4.tox2

3.1.1. Global mercury emissions

Total global mercury emitted in 2010 was 1772 t (metric tonnes), with the largest contribution from artisanal and small-scale gold mining (41.1%), followed by power generation (20.6%), cement production (8.6%), non-ferrous industry (7.5%), combustion in industry (6.6%), agricultural waste burning (5%), iron and steel (4.1%), combustion in residential (3.2%), solid waste incineration (1.9%), transport (1%) and chlor-alkali (0.5%) production using mercury cell technology. This updated version, as mentioned in section 2.1, provides improved emissions information for all sectors, not only for the more recent years but also going back to 1970; the sectors with significant changes in mercury emissions are agricultural waste burning, power generation and ASGM sectors. Consequently, in 2008 the total global Hg emission in EDGARv4.tox2 was 27% higher than in the previous version EDGARv4.tox1. Fig. Si3 of the Si illustrates the differences between the two EDGARv4 versions. Note that the relative differences increase over the period 1970–2012.

In EDGARv4.tox2 emissions of mercury species are calculated by multiplying Hg emissions with sector specific speciation factors from AMAP/UNEP (2008). The shares (%) for mercury species in total global Hg emission and Hg total, Hg^0, Hg^{2+} and Hg-P emission trends are illustrated in Fig. 2. The global trend of Hg^0 is driven by emissions from the ASGM sector. In the 1970s, the share of Hg^0 was approximately 60% and it increases over time, reaching 74% in 2005 and 75% in 2010. Consequently, the shares in total global Hg emission of reactive mercury forms, which are more fuel combustion driven have declined, for Hg^{2+} from 32% in 1970s to 20% in recent years and for Hg-P from 8% to 5.5%.

3.1.2. Emissions of reactive mercury in the three ex-post scenarios

In EDGARv4.tox2_S1, emissions of reactive mercury forms, i.e., Hg^{2+} and Hg-P, accounted for 25.3% of total global Hg emissions in 2010, equivalent to 447 t. In the other two scenarios reactive mercury emissions are lower, 22.9% (406 t) for S2 and 21.4% for S3 (378 t). Note that in S1, S2 and S3 the total Hg emissions remain the same.

The emissions estimates of reactive mercury forms (Hg^{2+} and Hg-P) are presented in Fig. 4. As described, in S1 and S2 only the emissions from power generation are different; for the rest of the sectors there are no differences between the emissions of reactive mercury of S1 and S2. With a 10-year time step, the global total emissions of reactive mercury forms are illustrated in Fig. 4a. In 1970, 1980 and 1990, the S2 reactive mercury emissions are higher than those in S1 by approximately 24.8%, 22.2% and 11%, respectively, and in 2000 and 2010 are lower than those in S1 by approximately 1.5% and 23%, respectively, showing the effect of modern control device utilisation. For S3 reactive mercury emissions are lower than those in S1 and in S2 for all years although at sector level the variation could be different, e.g., for non-ferrous industry in 2010, emissions in S3 are higher than those in S1 and S2 by 107%. It is important to mention the fact that the ASGM sector releases only Hg^0; therefore, this sector is not contributing to the emissions of reactive mercury.

The trends for the countries that contribute most to the reactive mercury emissions are illustrated in Fig. 4b for China, Fig. 4c for India and Fig. 4d for the United States. The power generation sector is an important contributor in all of these countries. In China, industry sector and cement production also have a greater share in national total emissions of reactive mercury forms and in India, agricultural waste burning emissions in S1 and S3 and industry in all scenarios together with power generation drive the trends.

Looking at the iron and steel industry and power generation sectors in more detail as these are the sectors affected most by the different

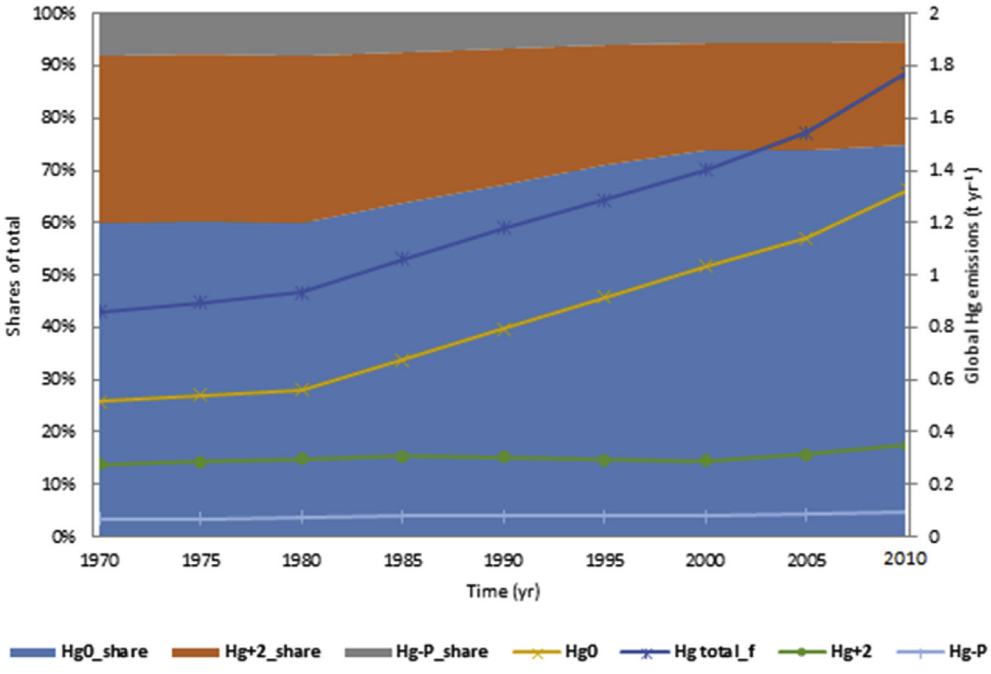

Fig. 2. EDGARv4.tox2 - shares and global emissions of total mercury and mercury species [tonne/yr].

speciation scenarios. For the iron and steel industry for example in China, the shares of reactive mercury forms in total mercury emissions in 2012 are 20% for S1 and 69.9% for S3, which results in a 17.3 t difference between S3 and S1 (Fig. Si5). For power generation, this can be quantified per fuel type, combustion technology and control measure system. In South Africa, for public electricity production, bituminous coal combusted in a pulverized coal dry bottom boiler, these shares are 50% for S1, 67% for S2 and 40% for S3, which lead to 1.62 t/yr difference between S2 and S1, and -0.95 t/yr difference between S3 and S1. In Fig. Si6 the variations in emissions of mercury forms from 1970 until 2012 are illustrated for this case considering also emissions associated to existing EoPs. With these findings, we demonstrate that the assumptions used in this study to estimate emissions of mercury species are key elements that drive the changes in the quantities of anthropogenic reactive mercury emissions to the atmosphere for each of the scenarios. Consequently, the impacts of mercury emissions at the regional and global scales estimated by chemical transport models are strongly affected by the input data provided by these scenarios.

3.1.3. Emissions distribution and global grid-maps

In EDGARv4.tox2, technology-based activity data, and emission factors and information on control measures were used to estimate mercury emissions as country totals for each key emitting sector. This inventory provides, for all world countries, emissions time series from 1970 to 2012. Additionally, using the methodology described in Muntean et al. (2014), mercury emissions were distributed at the places from where they are emitted using proxy data. Compared to EDGARv4.tox1, in EDGARv4.tox2 the proxy used to create emissions grid-maps have been updated for the power generation, industrial activities, gas and oil production and cement production. Details about the new updated proxy in EDGAR are provided in Janssens-Maenhout et al. (2017).

Continuous improvement of proxy data leads to a better emissions distribution of anthropogenic mercury emissions on the grid-maps and consequently enhances the quality of the input to chemical transport models. Global mercury emissions in EDGARv4.tox2 are distributed on $0.1^0 \times 0.1^0$ resolution grid-maps. These global grid-maps are available for all the sectors and years, for total Hg and mercury species. Fig. 3 shows the areas with elevated mercury emissions on global grid-map for 2012; all mercury-emitting sources are included. Grid-maps are also provided for the three ex-post emissions scenarios that we analysed in this study (see section 6).

The differences in emissions when gridded for S3 vs S1 and S2 vs S1 are shown in Fig. 4e and Si4 respectively for 2010. In Fig. 4e, in red are locations where the emissions in S3 are higher than those in S1 are, and in blue are those locations for which the emissions are lower. The difference between total emissions of reactive mercury forms in S2 and S1 is represented in Fig. Si4 of the Si.

3.1.4. EDGARv4.tox2 mercury emissions inventory comparison with other emissions inventories

As illustrated in Fig. Si3 and described in section 2.1, the changes in EDGARv4.tox2 are primarily related to agricultural waste burning, power generation, ASGM and solid waste incineration. These improvements give higher global mercury emissions in tox2 compared to tox1. In this section, we provide a comprehensive comparison with the global mercury emissions inventory developed by UNEP and presented in its reports (UNEP, 2013a; c). Sectorial comparison of UNEP vs EDGARv4.tox2 worldwide anthropogenic emissions of mercury to the atmosphere for the year 2010 is presented in Fig. 5. In these emissions inventories, for the matching sectors only, the totals are 1578.1 t for EDGARv4.tox2 and 1779.9 t for UNEP. The EDGARv4.tox2 is 10% lower than UNEP inventory, but it is well within the range reported by UNEP for which the lower and upper bounds are 899.9 t and 3584.5 t. At the sector level, for coal combustion in power generation, industry and residential EDGARv4.tox2 is 2.1% higher than UNEP mercury emission; mercury emission from bio, waste, gas and liquid fuels, which represents 194 t in total EDGARv4.tox2 emissions, are not included in this comparison. Mercury emissions of EDGAR, for the rest of the sectors, are within UNEP sectoral ranges except for chlor-alkali production using mercury cell technology and mercury mining for which mercury emissions in EDGARv4.tox2 are lower than UNEP lower bounds for these activities. However, the latter two sectors have low shares of total global mercury emissions, i.e., 1% and < 1%, respectively (UNEP,

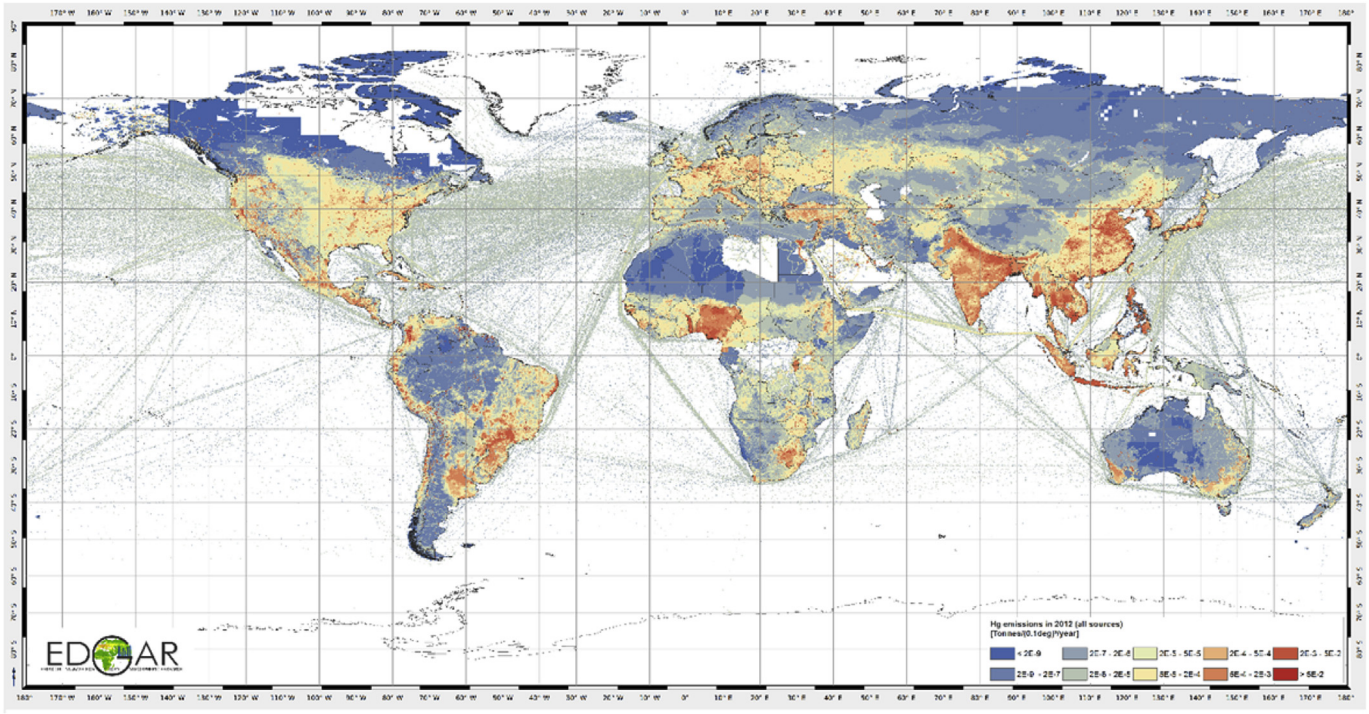

Fig. 3. EDGARv4.tox2 – mercury emissions gridmap at 0.1° × 0.1° resolution for 2012, all sources included.

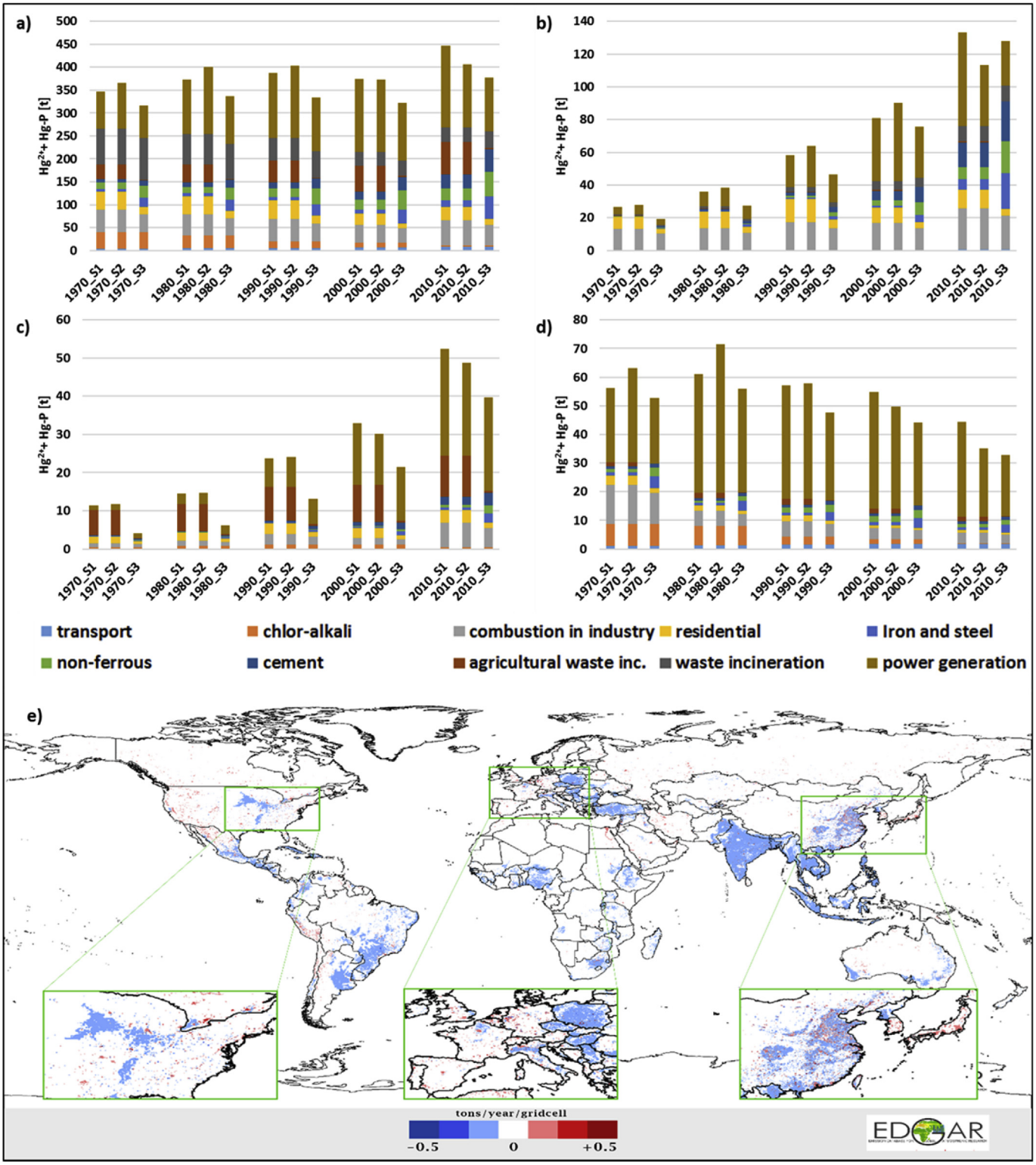

Fig. 4. Emissions of reactive mercury forms by sector in scenario S1, S2 and S3: a) global, b) China, c) India and d) the United States. In panel e), the difference between total emissions of reactive mercury forms in S3 and S1 is represented on global scale gridmap for 2010.

2013c), and are not expected to influence the overall results. The levels of emissions from ASGM are comparable, since both inventories used the same data sources for their estimations.

Comparison with national emissions inventories is much more challenging due to the differences in sub-sector aggregation and approaches used to estimate emissions. Among the world's countries, China is the largest contributor to the total mercury emissions, e.g., the share in 2010 was 29.7%. In this study, we performed an in-depth comparison between aggregated sectors as they are aggregated in each emissions inventory, analysing not only the emissions levels but also the differences in AD, EF and EoP. Table Si3 illustrates the full comparison for the year 2010 between EDGARv4.tox2 mercury emissions for China and the national mercury emissions inventory (China-NEI) developed by Zhao et al. (2015).

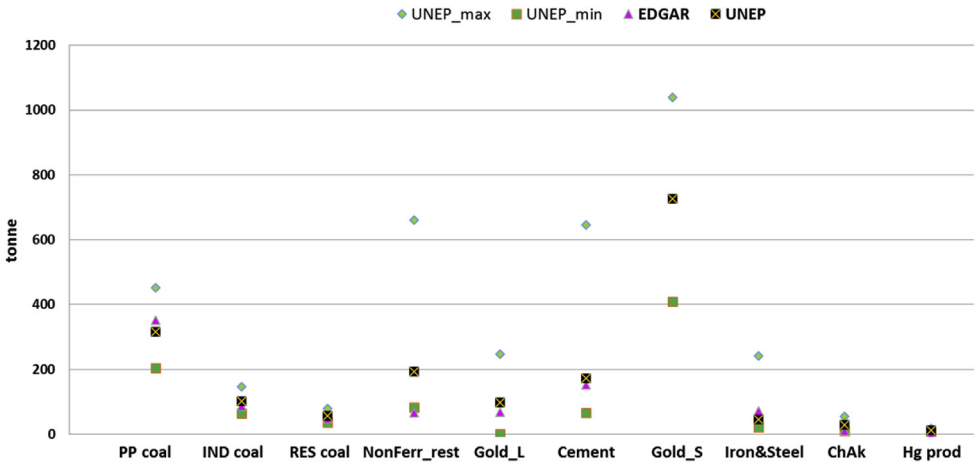

[1]Where "PP coal" represents mercury emissions from coal combustion in power generation, "IND coal" from coal combustion in industry, "RES coal" from coal combustion in residential and others, "NonFerr_rest" from Zinc, Lead and Copper production (in UNEP emission inventory mercury emission from aluminum production, "Gold_L" from large scale gold production, "Cement" from cement production, "Gold_S" from ASGM, "Iro&Steel" from iron and steel industry, "ChAk" from chlor-alkali production using mercury cell technology and "Hg prod" from mercury mining production.

Fig. 5. Global Mercury emissions comparison by sector[1], 2010: UNEP vs EDGARv.tox2. The emissions from Gold_S sector in EDGAR and UNEP inventories are comparable. (For interpretation of the references to color in this figure legend, the reader is referred to the Web version of this article.)

Since not all the sectors/aggregated sub-sectors in the two emissions inventories are fully matching, we discuss here only the differences and the steps forward to improve the EDGAR mercury emissions inventory. The total mercury reported emissions in China-NEI is 43% higher than the total emissions in EDGARv4.tox2. Sectors not matching are "battery/fluorescent lamp production" and "PVC production", which are included only in China-NEI, and "oil, gas, biomass and waste combustion in power generation" and "glass production" that are included only in EDGARv4.tox2. The sectors with partial matching are combustion in industry and residential; for these sectors the emissions in China-NEI are 2.3 times higher than the emissions in EDGARv4.tox2. For zinc production, for which the ADs are comparable in the two emissions inventories, the implied emission factor in China-NEI is 2.7 times higher than the EF (EMEP/EEA, 2013) used in EDGARv4.tox2. The emissions are also different for lead and copper production, mainly because in China-NEI both are considered primary (ores smelting) and secondary (scrap smelting) processes, whereas in EDGARv4.tox2, the EMEP/EEA (2013) provides EFs only for mercury emissions from primary lead and copper processes. For cement production, China-NEI takes into consideration the fast penetration of EoPs after 2008 in this sector, whereas in EDGARv4.tox2, we consider only the decrease in clinker content in cement in later years (Fig. Si2). Consequently, for cement production in 2010, EDGARv4.tox2 was 1.6 times higher than China-NEI, although in 2007, the levels of emissions from this sector were comparable. However, to gain further insights in the causes of these differences, a harmonised sectorial aggregation of activity data is needed, along with a better matching and further analysis on the national EFs derived from field measurements.

For the activities which match well in both inventories, such as coal combustion in power generation, solid waste incineration, iron and steel plants and gold production, the respective mercury emissions in China-NEI are 15%, 9%, 8% and 2% higher than those in EDGARv4.tox2. Although EDGARv4.tox2 provides global mercury emissions that are based on the independent international statistics, for AD and official EFs datasets, adjustments need to be made when reliable information from countries with large contributors is available. The outcome of continuous efforts to assimilate the advancement of knowledge for a better evaluation of mercury emissions is illustrated also by Wu et al. (2016) for China. The levels of mercury emissions estimated in his study for the year 1999 are about 30% lower than the value provided by Streets et al. (2005), and for the year 2003 are about 32% lower than the value provided by Wu et al. (2006) and 9% higher than the evaluation of Zhang et al. (2015).

3.2. Mercury wet deposition in ex-post emission scenarios

As described in Section 3.1.2, different assumptions of mercury speciation factors in the three ex-post emissions scenarios lead to considerable differences in reactive mercury emissions estimates as well as their spatial and temporal distributions. In order to evaluate their impacts on the global and regional cycles of mercury, global and nested grid (over North America) simulations of GEOS-Chem are conducted using anthropogenic emissions from these three ex-post emissions scenarios (see Section 2.3) for an example period of 2010–2012. The wet deposition fluxes of total reactive mercury (Hg^{2+} and Hg-P) are averaged between 2010 and 2012, to remove variability not resolved by our model. Note that the differences in wet deposition between the scenarios described below are only representative of this period. Model simulation results are compared with the observed wet deposition fluxes of total reactive mercury (Hg^{2+} and Hg-P) but not with the atmospheric concentrations of reactive mercury species due to the high bias and/or uncertainty associated with these measurements (Jaffe et al., 2014). Specifically, wet deposition observational data from the United States National Atmospheric Deposition Program (NADP) Mercury Deposition Network (MDN; http://nadp.sws.uiuc.edu/mdn/) are used here, which includes about one hundred monitoring stations. Mercury wet deposition observations are still relatively sparse at other regions.

The differences in simulated deposition between S1, S2, and S3 indicate that speciation factors can drive changes in wet deposition of ± 10%, and in some cases, close to 20% (see Fig. Si9 for difference plots as percent change). At the global scale, the difference between the wet deposition fluxes in S2 and S1 is presented in Fig. 6c (shown in μg m^{-2} yr^{-1}). For S2, wet deposition fluxes are lower than those in S1 in parts of China, India, Europe and the United States. The largest differences of about -3.4 μg m^{-2} yr^{-1} are found in eastern and central China where many coal-fired power plants are located (and assumption included in S2 makes a big difference). As described above, in S1 and S2 only the emissions from power generation are different and that the mercury speciation splitting factors are from AMAP/UNEP (2008) and EPA's ICR (Bullock and Johnson, 2011) for S1 and S2, respectively. Therefore, compared to S1 (reference scenario), the lower reactive

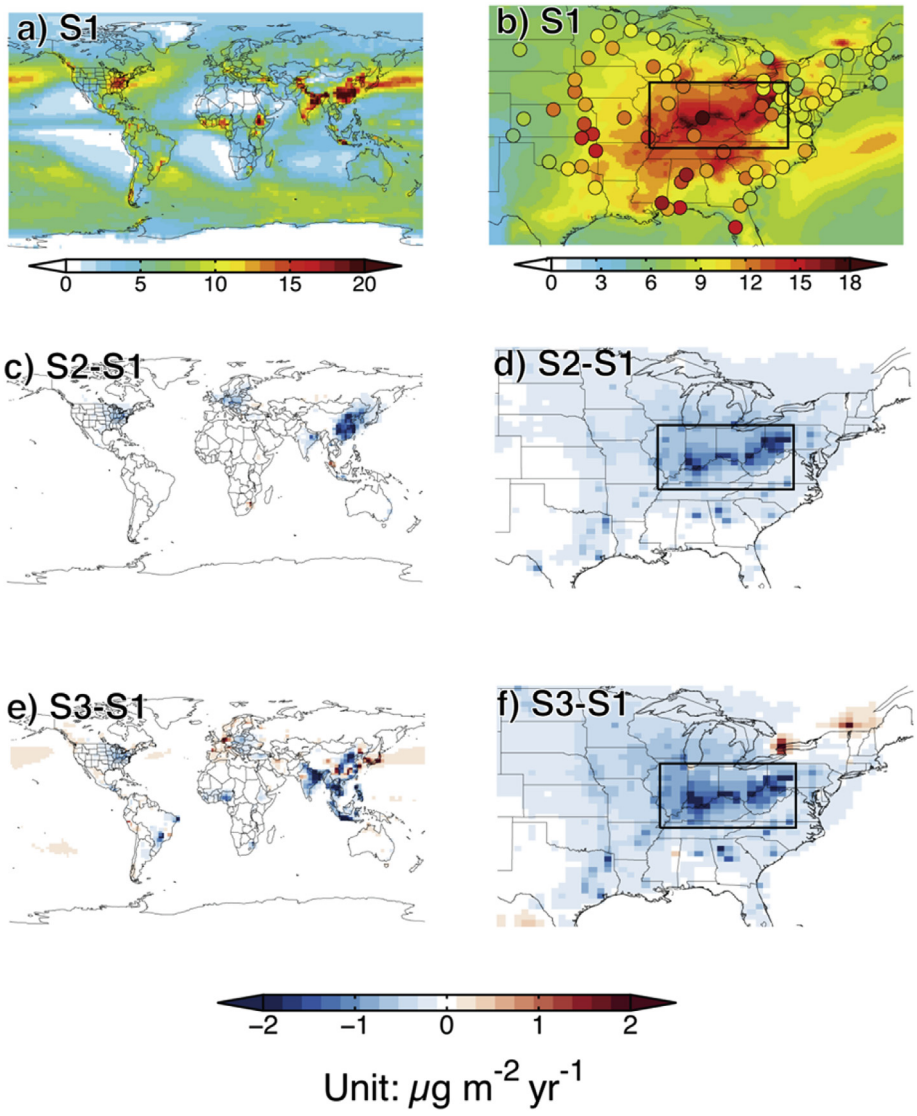

Fig. 6. Wet deposition fluxes of total reactive mercury (Hg^{2+} and Hg-P), averaged between 2010 and 2012 [$\mu g\ m^{-2}\ yr^{-1}$]. a), c) and e) are global maps showing S1, the difference between S2 and S1, and the difference between S3 and S1, respectively. b), d) and f) are the maps over the eastern United States showing S1, the difference between S2 and S1, and the difference between S3 and S1, respectively. The colored circles in b) represent the wet deposition flux observations from Mercury Deposition Network (MDN). The black-line rectangle in b), d) and f) indicate the ORV (Ohio River Valley) region.

mercury emissions from power generation (see Fig. 6 and Fig. Si7) result in smaller wet deposition fluxes in the aforementioned regions. Fig. 6e presents the difference between the wet deposition fluxes in S3 and S1. The mercury speciation factors for mercury emitting sectors are obtained from recently published studies in S3. For S3, wet deposition fluxes are lower over certain regions in China, India, Southeast Asia, and the US, but are higher over some regions in west Europe. The modelled spatial distribution of the difference between the wet deposition fluxes largely reflects the distribution from reactive mercury emissions (see Fig. 4).

As shown in Figs. 6d and S2 has reduced wet deposition fluxes over the eastern United States in 2010–2012, when compared to S1 (reference scenario). The reduction is more obvious in the Ohio River Valley (ORV) region (as large as about 2.4 $\mu g\ m^{-2}\ yr^{-1}$ or 13%) where many coal-fired power plants are located. The difference between the wet deposition fluxes in S1 and S2 results from the different speciation factors of mercury from the power generation sector, suggesting less emissions in reactive mercury forms over this region (see Fig. 6d). When compared to S1, S3 has reduced wet deposition fluxes (in the range of 5–15%) in some parts of the eastern United States in 2010–2012 but enhanced fluxes (of up to 2 $\mu g\ m^{-2}\ yr^{-1}$, or 12%) in some others, like southern Ontario and Quebec in Canada (see Fig. 6f). The more scattered spatial patterns are because the speciation factors in multiple residential and industrial sectors (and EoPs) are changed; for instance, changes to speciation factors for metal smelting that shift emissions towards reactive species result in the increased deposition in south eastern Canada. For S3, the ORV region also shows reductions in wet deposition fluxes compared to S1 that are similar in magnitude to S2.

We compare the modelled and MDN-observed wet deposition fluxes over the eastern United States averaged over 2010–2012 (see Fig. 6b and Fig. Si7). There are 11 stations in the Ohio River Valley region and 67 stations elsewhere. Considering all 78 stations, the average wet deposition flux in the three scenarios (S1: 9.8, S2: 9.4 and S3: 9.4 $\mu g\ m^{-2}\ yr^{-1}$) are similar and somewhat lower than that observed by MDN (10.3 $\mu g\ m^{-2}\ yr^{-1}$). However, in the Ohio River Valley region (11 stations), the three scenarios (S1: 14.0, S2: 12.9 and S3: 13.0 $\mu g\ m^{-2}\ yr^{-1}$) overestimate the average wet deposition flux observed by MDN (11.4 $\mu g\ m^{-2}\ yr^{-1}$) by 23%, 13% and 14%, respectively. Therefore, applying S2 and S3 emissions of reactive mercury

may better simulate the wet deposition in the Ohio River Valley region.

3.3. Uncertainties

Caution is required when interpreting results of the model-to-observation comparisons. Significant uncertainties exist in both the MDN observations and GEOS-Chem model results of wet deposition fluxes. The uncertainties in the observed wet deposition fluxes are estimated to be approximately 10% (Prestbo and Gay, 2009). The model suffers from (1) an incomplete understanding of atmospheric chemistry mechanisms involving both oxidation of Hg^0 and reduction of reactive mercury (Ariya et al., 2015), (2) an unclear partitioning mechanism of reactive mercury between the gas and particulate phases (Rutter and Schauer, 2007), (3) insufficient horizontal/vertical resolution in representing the atmosphere, and (4) the simulated precipitation and mercury scavenging by stratiform and convective precipitation systems (Holmes et al., 2016).

The uncertainties in the emissions inventory are those presented and discussed by Muntean et al. (2014). The ASGM sector, which has a significant contribution to the global mercury emissions, is characterized by large uncertainty; however, in EDGARv4.tox2, an improvement can be seen for this sector for which more information and data are collected by AGC (see Fig. 7c). An additional source of uncertainty is the contribution of mercury-containing commercial products (e.g. batteries) to anthropogenic emissions of Hg^0 (Horowitz et al., 2014; Zhang et al., 2016), which have been estimated to account for on the order of 400 t of emissions in 2010 (Zhang et al., 2016). The addition of a large additional source of Hg^0 emissions based on inventories from Zhang et al. (2016), does not change the spatial pattern of simulated wet deposition. It does however enhance the magnitude of wet deposition, particularly in areas where wet deposition is driven by atmospheric oxidation of Hg^0 to divalent mercury (Hg^{2+}), rather than locally/regionally emitted divalent mercury. Thus, while the contribution of mercury-containing products remains an important area for further investigation in inventory development, it does not substantially affect our findings on regional wet deposition patterns.

4. Discussion

Anthropogenic mercury emissions are key to understanding the atmospheric mercury cycle. The accuracy of their estimation is essential for impact evaluation using transport and chemical models and further to decide on mitigation actions and measure their effectiveness. Inverse modelling (Song et al., 2015) has shown that optimised anthropogenic emissions of Hg^0 for Asia are higher than bottom-up estimates of anthropogenic mercury; these findings indicate the need to improve emissions inventories, not only for total Hg but also for mercury species in general.

In this section, we discuss the variation in emissions trends over years, highlighting in particular the changes in mercury emissions from the ASGM sector, and we examine region specific mercury speciation footprints.

4.1. Global trends in mercury emissions of fast changing sectors over more than forty years

The EDGARv4 global mercury emissions inventory is continuously updated with the emissions from the most recent years and improved for historical reconstructions by using the most recent knowledge and data sources on AD, EFs and EoPs; the tox2 version contains recent updates and improvements as described in section 2.1. Fig. 7a illustrates the levels of mercury emissions for each sector, except ASGM, over more than forty years. Since 1970, the mercury emissions from waste incineration, combustion in industry and residential, and chlor-alkali production using mercury cell technology sectors have decreased by 6%, 5% and 94%, respectively.

This was offset by the increases in emissions from fast-growing sectors such as cement production, metal industry (w/o ASGM), power

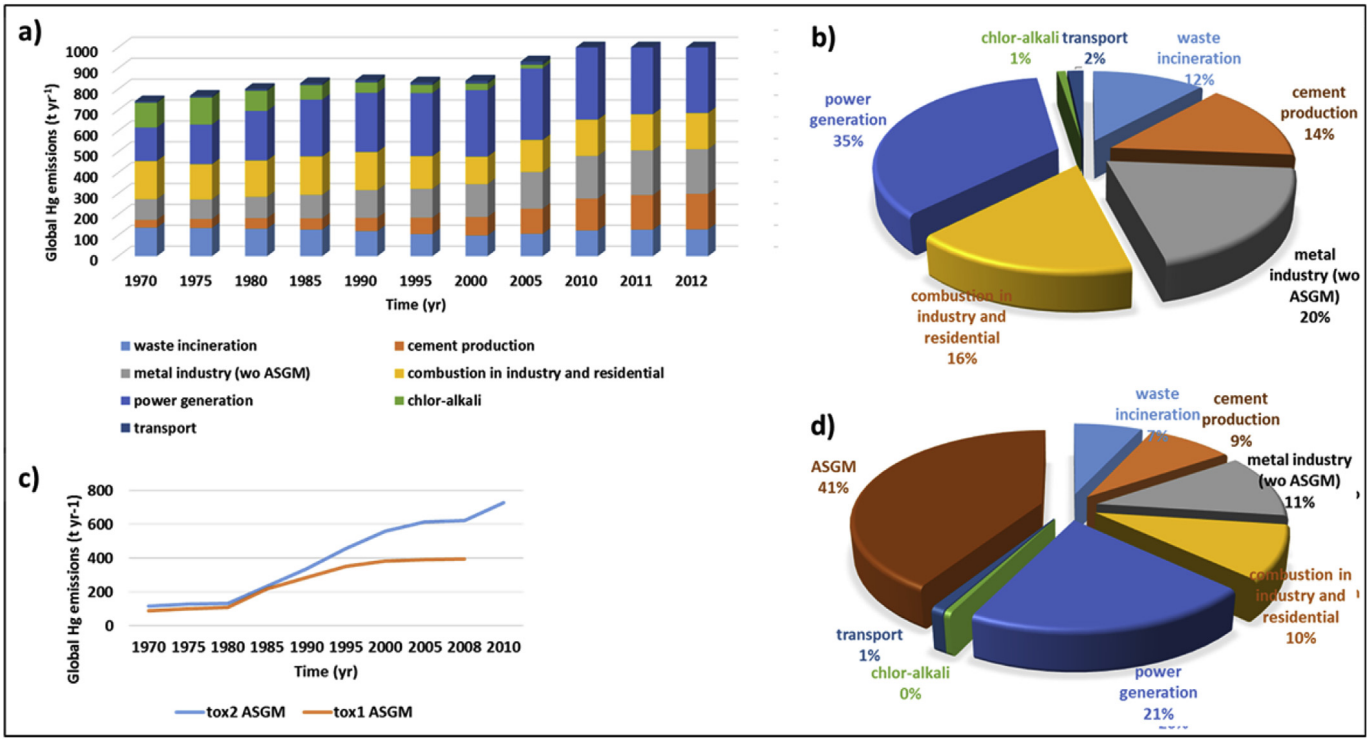

Fig. 7. EDGARv4.tox2 global mercury emissions by sector. Panel a) global mercury emission trends over more than forty years by sector (emissions from AGSM not included), panel b) sectoral emissions breakdown in 2010 excluding artisanal and small-scale gold mining (ASGM), panel c) trends of mercury emissions from ASGM sector in tox1 and tox2 EDGARv4 versions, panel d) sectoral emissions breakdown in 2010 including ASGM. (For interpretation of the references to color in this figure legend, the reader is referred to the Web version of this article.)

generation and transportation by 361%, 115%, 129% and 135%, respectively. These sectorial emissions changes resulted in an increase in total global mercury emissions from these sectors by 45% in 2012 compared to those in 1970. A sectorial breakdown for the year 2010 of mercury emissions apart from ASGM is presented in Fig. 7b. Power generation produces 35% of the total non-ASGM global mercury emissions followed by the metal industry (w/o ASGM) with 20%, combustion in industry and residential (16%), cement production (14%), waste incineration (12%), transportation (2%) and chlor-alkali (1%).

Mitigation of mercury emissions in the ASGM sector is expected to be significant in the upcoming years considering the provisions of the Minamata Convention (UNEP, 2013b) related to this activity. In many countries, ASGM activities are illegal. The data on mercury consumption and technologies used by these activities, that are needed to evaluate emissions tend to be scarce, with limited coverage and available only for the last few years; consequently, the uncertainty in mercury emissions estimation from this sector is and will probably remain large. The evaluation of mercury emissions from ASGM from 1970 until 2012 in EDARv4.tox2 is based on the methodology described by Muntean et al. (2014), in which the gold market demand is assumed to be the only driver of mercury emissions from this sector. Fig. 7c illustrates the differences in mercury emissions, tox2 vs tox1, in which we used as input data from AGC (2010a) and Telmer K and Veiga M (2008), respectively, to estimate mercury emissions. The use of a more complete and recently updated data source (AGC, 2010a) resulted in 32% higher emissions in tox2 compared to tox1 in 1970, 18% in 1990 and 57% in 2008.

As illustrated in Fig. 7d, by adding ASGM to the other key mercury emissions sources, the breakdown of mercury emission in 2010 will be: ASGM contributing 41%, power generation 21%, metal industry (wo ASGM) 11%, combustion in industry and residential 10%, cement production 9%, waste incineration 7%, transport by 1% and chlor-alkali < 1%. Because the ASGM sector has an important share in total global mercury emissions and in driving the global trends, improvements in mercury emissions estimation for this sector are needed.

4.2. Region specific mercury emission speciation footprints

With information and EFs derived more from field measurements, both modelled scenarios (S2 and S3) highlight the real-world variations that occur between and within emissions sectors due to differential application of air pollution control devices, differences in fuel type and composition and operating procedures. The widespread application of EoPs may result in lower reactive mercury emissions (as we can see from recent literature (S3) and the EPA's ICR (S2)) compared to the 50/50 of reactive mercury (Hg-P + Hg^{2+})/Hg^0 shares in AMAP/UNEP (2008). A short review of how these factors affect emissions speciation is provided in the Si. Table Si4 provides, for the year 2010, emissions of Hg, Hg-P + Hg^{2+} and their shares in total global Hg and in total global reactive mercury emissions (called hereafter Reg_share_Hg and Reg_share_reactive, respectively) for 24 world regions, which are defined in the IMAGE model (Bouwman et al., 2006), and for international shipping. Knowing that the reactive mercury is emitted primarily from combustion processes, we can distinguish between the regions with larger contributions to mercury emissions from combustion processes. The higher the Reg_share_reactive the more regional/local deposition we can expect. For example, for the top contributors to the global mercury emissions, the Reg_share_Hg and Reg_share_reactive (S1) are 30.2% and 30.9% for China, 6.6% and 12.5 for India, and 5.5% and 12.5% for the USA, respectively, whereas the values for Rest of South America are 11.5% and 2.2%. Extended information on the speciated mercury emissions regional footprint for the period 1970–2010 is provided in Fig. Si8 for all scenarios.

The modelled scenarios suggest that the impacts of speciation on wet deposition are mostly likely to be observed directly downwind of source regions, with much more diffuse effects observed in areas where wet deposition is primarily influenced by global background concentrations of Hg. For instance, in our high resolution regional simulations over the US, differences between speciation scenarios are larger over the Ohio River Valley (where many emissions sources are located) than when considering a larger area with all MDN stations. Additional monitoring of wet deposition downwind of sources is thus needed to better constrain speciation from sectors where uncertainty is the largest, like metals industries. While these scenarios do not capture the full range of global variability, they illustrate that regional differences in technology, fuel content and type, and operating procedures that have implications for speciation. The results underscore the need for regionally specific field measurements to derive region-specific EFs, particularly in Central and South America, Africa, and the Middle East. Further, they underscore that mercury pollution is not only a global, but also a regional and local issue, and that local-scale impact evaluations will require detailed measurement information on emissions speciation.

5. Conclusions

Mercury species emitted in the atmosphere are deposited locally or transported long distances, and bioaccumulate; this could damage the environment and depending of the level and the route of exposure (e.g. diet, inhalation) mercury could affect human health. More accurate emissions evaluation, in particular for mercury species emitted from the ASGM, combustion and metal industry, could lower the uncertainty of the input to the chemical transport models and consequently contribute to the improvements of the impact evaluation of anthropogenic mercury emissions at both regional/local and large scales.

The outcome of this research is a step forward in the process of improving the evaluation of local impacts of mercury emissions by using different mercury emissions estimations, focusing on reactive species in particular, as input for global and nested simulations. We varied emissions of mercury species in total Hg by applying different speciation factors and presented the resulted emissions in three retrospective scenarios. For the metal industry, when compared to reference scenario, i.e., S1 (speciation factors from AMAP), the levels of reactive mercury emissions are higher in the global inventory of S3 (speciation factors from recent scientific publications). In scenario S3, we used activity-specific speciation factors for each sub-sector with reactive mercury shares varying in the range between 50% and 68%, whereas for S1 a share of 20% was used for all the activities in metal industry sector. For cement production, the reactive mercury shares used in this study are 32% in S3 and 20% in S1. On the other hand, for combustion in residential, industry and power generation, in S1 the share of reactive mercury is 50%, in S3 instead we used lower shares that varied from 17% to 26% for residential, from 26% to 39% for industry and from 15% to 50% for power generation. In scenario S2 (speciation factors from EPA's ICR for power generation and from AMAP from the rest of the sectors), which includes the speciated emissions from S1 for all sectors except power generation, the shares of reactive mercury emissions associated to different fuel, technology and EoPs in power generation are in the range between 4% and 85%. These significant differences between the amounts of mercury species in anthropogenic mercury emissions of S1, S2 and S3 inventories influence the scale-related impacts of these emissions. Findings from nested simulations with GEOS-Chem model over the United States, in the Ohio River Valley where most of the power plants are located, show that reactive mercury emissions are producing impacts that are sensitive to the variations of emissions speciation factors for the total Hg. Further, regional characteristics of wet deposition induced by mercury species emissions from different industries are seen on the maps from global simulations. Equally important is to investigate also the changes in TGM (total gaseous mercury, Hg^0 and Hg^{2+}) using retrospective mercury speciation emissions scenarios as input to chemical transport models and compare modelled concentrations with available observational data;

this is not the goal of this paper.

In this study, we describe the EDGARv4.tox2 and provide both emissions time series from 1970 to 2012 and global grid-maps for this global gridded anthropogenic mercury emissions inventory. We provide a comprehensive comparison by sector of EDGARv4.tox2 with the UNEP Minamata global estimates and with national emissions of China, which is the largest contributor to the global total mercury emissions. This comparison shows a good agreement with the emissions inventory of UNEP (2013c) while for the national China-NEI greater harmonisation of sources classification is needed to a better sector-matching between the two emissions inventories. For lead and copper production, the China-NEI does not distinguish between primary and secondary production and in EDGARv4.tox2, emissions are estimated only for primary processes. Instead, for combustion in residential and industry more details are needed for a meaningful comparison. For power generation we used country specific information to update the EoPs in EDGARv4.tox2 but given the extensive investments in the latest years, which are targeting also emissions mitigation in China (Zhao et al., 2015), the emissions from other sectors such as cement production and metal industry are cut down despite production increases. Field emissions measurements, which are, to some extent, available for countries that contribute most to mercury emissions such as China (Wang et al., 2010), are seen as a benefit to the emissions estimation leading to a more realistic approach.

We provide a detailed gridded inventory at $0.1 \times 0.1^{\circ}$ resolution of mercury species including region-specific information over forty years emphasising which sectors are relevant and adding knowledge to support possible regional mercury emissions reduction schemes. In this study, however, we demonstrated that the proportion of mercury species shows variation from one scenario to another, which lead to the conclusion that more precise speciated mercury splitting factors, e.g. derived from field measurements, associated to different activities are needed. We envisage updates of speciation factors for each sector based on reliable scientific information, which will be implemented in the next.tox version of EDGAR. This will emphasize better the impacts of EoPs and technology penetration on mercury species emissions. Despite the time lag between implementation of the mitigation measures and their description in scientific literature, special attention will be given to these changes in the fast growing economies that contribute most to the mercury emissions. In addition, further research could be added to this work e.g. oriented towards more accurate emissions inventories of mercury species to be used as input for nested simulations over other areas with elevated mercury emissions within which also the wet depositions and concentrations of mercury are measured.

Even though the separate mercury species are not explicitly mentioned in Minamata Convention (Selin, 2014), it relies on underlying knowledge on the environmental mercury cycle and long-range transport and deposition. This study contributes to this knowledge base by shedding light on the impacts of mercury emission speciation ex-post scenarios on modelled global and regional wet deposition patterns.

Data availability

The EDGARv4.tox2 mercury emission global grid-maps are provided at http://edgar.jrc.ec.europa.eu/overview.php?v=4tox2 in netCDF ($kg/m^2/s$) and.txt (t/cell) formats. Here, global grid-maps of total Hg and mercury species: Hg^0, Hg^{2+} and Hg-P are publicly available that can be freely downloaded, including the emissions grid-maps for EDGARv4.tox2_S1, S2 and S3. The EDGARv4.tox2 contains the latest updates and is consistent with EDGARv4.3.2 whereas EDGARv4.tox2_S1 is an earlier version that we used to develop mercury species emissions scenarios.

Acknowledgments

The views expressed here are purely those of the authors and may not be regarded as an official position of the European Commission or of any other research institutions.

We acknowledge support from the U.S. National Science Foundation, Atmospheric Chemistry Program under grant ##1053648 (NES and SS) and the Coupled Human and Natural Systems Program (NES and AG) #1313755\.

The authors would like to thank the anonymous reviewers for their valuable comments and suggestions to improve the quality of the paper.

Appendix A. Supplementary data

Supplementary data related to this article can be found at http://dx.doi.org/10.1016/j.atmosenv.2018.04.017.

References

AGC, 2010a. Global Database on Mercury Emissions from Artisanal and Small Scale Mining (ASGM). Artisanal Gold Council info retrieved from: www.mercurywatch.org [on 15 October 2013].

AGC, 2010b. Global Database on Mercury Emissions from Artisanal and Small Scale Mining (ASGM). Artisanal Gold Council info retrived from: www.mercurywatch.org [on 15 October 2013].

AMAP/UNEP, 2008. Technical Background Report to the Global Atmospheric Mercury Assessment. Arctic Monitoring and Assessment Progamme/UNEP Chemicals Branch.

Amos, H.M., Jacob, D.J., Holmes, C.D., Fisher, J.A., Wang, Q., Yantosca, R.M., Corbitt, E.S., Galarneau, E., Rutter, A.P., Gustin, M.S., Steffen, A., 2012. Gas-particle partitioning of atmospheric Hg (II) and its effect on global mercury deposition. Atmos. Chem. Phys. 12, 591–603.

Ariya, P.A., Amyot, M., Dastoor, A., Deeds, D., Feinberg, A., Kos, G., Poulain, A., Ryjkov, A., Semeniuk, K., Subir, M., Toyota, K., 2015. Mercury physicochemical and biogeochemical transformation in the atmosphere and at atmospheric interfaces: a review and future directions. Chem. Rev. 115, 3760–3802.

Bouwman, A.F., Kram, T., Goldewijk, K.K., 2006. Integrated Modelling of Global Environmental Change. An Overview of IMAGE 2.4. MNP publication number 5001 10002/2006. Netherland Environmental Assessment Agency, Bilthoven.

Bullock, D., Johnson, S., 2011. Electric Generating Utility Mercury Speciation Profiles for Clean Air Mercury Rule, EPA-454/R-11–1010. EPA.

Chen, L., Liu, M., Fan, R., Ma, S., Xu, Z., Ren, M., He, Q., 2013. Mercury speciation and emission from municipal solid waste incinerators in the Pearl River Delta, South China. Sci. Total Environ. 447, 396–402.

CSI, 2016. Cement sustainability initiative. Getting the numbers right (GNR) database. Internet: http://www.wbcsdcement.org/GNR-2012/index.html.

de Foy, B., Heo, J., Schauer, J.J., 2014. Estimation of direct emissions and atmospheric processing of reactive mercury using inverse modeling. Atmos. Environ. 85, 73–82.

EMEP/EEA, 2013. EMEP/EEA air pollutant emission inventory guidebook. Technical report No 12/2013. http://www.eea.europa.eu/publications/emep-eea-guidebook-2013.

FAO, 2015. Food and agriculture organization of the united Nations. http://www.fao.org.

Friedli, H.R., Radke, L.F., Lu, J.Y., 2001. Mercury in smoke from biomass fires. Geophys. Res. Lett. 28.

Friedli, H.R., Radke, L.F., Lu, J.Y., Banic, C.M., Leaitch, W.R., MacPherson, J.I., 2003a. Mercury emissions from burning of biomass from temperate North American forests: laboratory and airborne measurements. Atmos. Environ. 37, 253–267.

Friedli, H.R., Radke, L.F., Prescott, R., Hobbs, P.V., Sinha, P., 2003b. Mercury emissions from the August 2001 wildfires in Washington State and an agricultural waste fire in Oregon and atmospheric mercury budget estimates. Global Biogeochem. Cycles 17.

Gharebaghi, M., Hughes, K.J., Porter, R.T.J., Pourkashanian, M., Williams, A., 2011. Mercury speciation in air-coal and oxy-coal combustion: a modelling approach. Proc. Combust. Inst. 33, 1779–1786.

Giang, A., Stokes, L.C., Streets, D.G., Corbitt, E.S., Selin, N.E., 2015. Impacts of the Minamata convention on mercury emissions and global deposition from coal-fired power generation in Asia. ES T (Environ. Sci. Technol.) 49, 5326–5335.

Gratz, L.E., Keeler, G.J., Marsik, F.J., Barres, J.A., Dvonch, J.T., 2013a. Atmospheric transport of speciated mercury across southern Lake Michigan: influence from emission sources in the Chicago/Gary urban area. Sci. Total Environ. 448, 84–95.

Gratz, L.E., Keeler, G.J., Morishita, M., Barres, J.A., Dvonch, J.T., 2013b. Assessing the emission sources of atmospheric mercury in wet deposition across Illinois. Sci. Total Environ. 448, 120–131.

Holmes, C.D., Jacob, D.J., Corbitt, E.S., Mao, J., Yang, X., Talbot, R., Slemr, F., 2010. Global atmospheric model for mercury including oxidation by bromine atoms. Atmos. Chem. Phys. 10, 12037–12057.

Holmes, C.D., Krishnamurthy, N.P., Caffrey, J.M., Landing, W.M., Edgerton, E.S., Knapp, K.R., Nair, U.S., 2016. Thunderstorms increase mercury wet deposition. ES T (Environ. Sci. Technol.) 50 (17), 9343–9350.

Horowitz, H.M., Jacob, Daniel J., Amos, Helen M., Streets, David G., Sunderland, Elsie M., 2014. Historical mercury releases from commercial products: global environmental implications. ES T (Environ. Sci. Technol.) 48, 10242–10250.

IEA, 2014. International Energy agency. http://www.iea.org.

Jaffe, D.A., Lyman, S., Amos, H.M., Gustin, M.S., Huang, J., Selin, N.E., Levin, L., ter Schure, A., Mason, R.P., Talbot, R., Rutter, A., Finley, B., Jaeglé, L., Shah, V., McClure, C., Ambrose, J., Gratz, L., Lindberg, S., Weiss-Penzias, P., Sheu, G.-R.,

Feddersen, D., Horvat, M., Dastoor, A., Hynes, A.J., Mao, H., Sonke, J.E., Slemr, F., Fisher, J.A., Ebinghaus, R., Zhang, Y., Edwards, G., 2014. Progress on understanding atmospheric mercury hampered by uncertain measurements. Environ. Sci. Technol. 48, 7204–7206.

Jang, H.-N., Kim, J.-H., Jung, S.-J., Back, S.-K., Sung, J.-H., Kim, S.-H., Seo, Y.-C., Keel, S.-I., Liu, X., 2014. Mercury emission characteristics from coal combustion by supplying oxygen and carbon dioxide with limestone injection. Fuel Process. Technol. 125, 217–222.

Janssens-Maenhout, G., Crippa, M., Guizzardi, D., Muntean, M., Schaaf, E., Dentener, F., Bergamaschi, P., Pagliari, V., Olivier, J., Peters, J., van Aardenne, J., Monni, S., Doering, U., Petrescu, R., 2017. EDGAR v4.3.2 Global Atlas of the Three Major Greenhouse Gas Emissions for the Period 1970-2012. Earth System Science Data (ESSD).

Jongwana, L.T., Crouch, A.M., 2012. Mercury speciation in south african coal. Fuel 94, 234–239.

Kim, J.-H., Park, J.-M., Lee, S.-B., Pudasainee, D., Seo, Y.-C., 2010. Anthropogenic mercury emission inventory with emission factors and total emission in Korea. Atmos. Environ. 44, 2714–2721.

Liu, B., Keeler, G.J., Timothy Dvonch, J., Barres, J.A., Lynam, M.M., Marsik, F.J., Morgan, J.T., 2010a. Urban–rural differences in atmospheric mercury speciation. Atmos. Environ. 44, 2013–2023.

Liu, L., Duan, Y.-f., Wang, Y.-j., Wang, H., Yin, J.-j., 2010b. Experimental study on mercury release behavior and speciation during pyrolysis of two different coals. J. Fuel Chem. Technol. 38, 134–139.

Lyman, S., Gustin, M.S., Prestbo, E., Marsik, F., 2007. Estimation of dry deposition of atmospheric mercury in Nevada by direct and indirect methods. Environ. Sci. Technol. 41 (6).

Muntean, M., Janssens-Maenhout, G., Song, S., Selin, N.E., Olivier, J.G.J., Guizzardi, D., Maas, R., Dentener, F., 2014. Trend analysis from 1970 to 2008 and model evaluation of EDGARv4 global gridded anthropogenic mercury emissions. Sci. Total Environ. 494–495, 337–350.

Ochoa-González, R., Córdoba, P., Díaz-Somoano, M., Font, O., López-Antón, M.A., Leiva, C., Martínez-Tarazona, M.R., Querol, X., Fernández Pereira, C., Tomás, A., Gómez, P., Mesado, P., 2011. Differential partitioning and speciation of Hg in wet FGD facilities of two Spanish PCC power plants. Chemosphere 85, 565–570.

Omine, N., Romero, C.E., Kikkawa, H., Wu, S., Eswaran, S., 2012. Study of elemental mercury re-emission in a simulated wet scrubber. Fuel 91, 93–101.

Park, K.S., Seo, Y.C., Lee, S.J., Lee, J.H., 2008. Emission and speciation of mercury from various combustion sources. Powder Technol. 180, 151–156.

Prestbo, E.M., Gay, D.A., 2009. Wet deposition of mercury in the U.S. and Canada, 1996–2005: results and analysis of the NADP mercury deposition network (MDN). Atmos. Environ. 43, 4223–4233.

Rallo, M., Heidel, B., Brechtel, K., Maroto-Valer, M.M., 2012. Effect of SCR operation variables on mercury speciation. Chem. Eng. J. 198–199, 87–94.

Rutter, A.P., Schauer, J.J., 2007. The effect of temperature on the gas-particle partitioning of reactive mercury in atmospheric aerosols. Atmos. Environ. 41, 8647–8657.

Schleicher, N.J., Schäfer, J., Chen, Y., Blanc, G., Chen, Y., Chai, F., Cen, K., Norra, S., 2016. Atmospheric particulate mercury in the megacity Beijing: efficiency of mitigation measures and assessment of health effects. Atmos. Environ. 124 (Part B), 396–403.

Schofield, K., 2012. Mercury emission control from coal combustion systems: a modified air preheater solution. Combust. Flame 159, 1741–1747.

Selin, N.E., 2014. Global change and mercury cycling: challenges for implementing a global mercury treaty. Environ. Toxicol. Chem. 33, 1202–1210.

Selin, N.E., Jacob, D.J., Yantosca, R.M., Strode, S., Jaeglé, L., Sunderland, E.M., 2008. Global 3-D land-ocean-atmosphere model for mercury: present-day versus pre-industrial cycles and anthropogenic enrichment factors for deposition. Global Biogeochem. Cycles 22, GB2011.

Shah, V., Jaeglé, L., 2017. Subtropical subsidence and surface deposition of oxidized mercury produced in the free troposphere. Atmos. Chem. Phys. 17.

Sigler, J.M., Mao, H., Talbot, R., 2009. Gaseous elemental and reactive mercury in Southern New Hampshire. Atmos. Chem. Phys. 9, 1929–1942.

Soerensen, A.L., Sunderland, E.M., Holmes, C.D., Jacob, D.J., Yantosca, R.M., Skov, H., Christensen, J.H., Strode, S.A., Mason, R.P., 2010. An improved global model for air-sea exchange of mercury: high concentrations over the North Atlantic. Environ. Sci. Technol. 44, 8574–8580.

Song, S., Selin, N.E., Soerensen, A.L., Angot, H., Artz, R., Brooks, S., Brunke, E.G., Conley, G., Dommergue, A., Ebinghaus, R., Holsen, T.M., Jaffe, D.A., Kang, S., Kelley, P., Luke, W.T., Magand, O., Marumoto, K., Pfaffhuber, K.A., Ren, X., Sheu, G.R., Slemr, F., Warneke, T., Weigelt, A., Weiss-Penzias, P., Wip, D.C., Zhang, Q., 2015. Top-down constraints on atmospheric mercury emissions and implications for global biogeochemical cycling. Atmos. Chem. Phys. 15, 7103–7125.

Streets, D.G., Hao, J., Wu, Y., Jiang, J., Chan, M., Tian, H., Feng, X., 2005. Anthropogenic mercury emissions in China. Atmos. Environ. 39, 7789–7806.

Subir, M., Ariya, P.A., Dastoor, A.P., 2012. A review of the sources of uncertainties in atmospheric mercury modeling II. Mercury surface and heterogeneous chemistry – a missing link. Atmos. Environ. 46, 1–10.

Tang, S., Wang, L., Feng, X., Feng, Z., Li, R., Fan, H., Li, K., 2016. Actual mercury speciation and mercury discharges from coal-fired power plants in Inner Mongolia, Northern China. Fuel 180, 194–204.

Telmer, K., Veiga, M., 2008. World emissions of mercury from artisanal and small scale gold mining. In: Pirrone, N., Mason, R. (Eds.), InterimReport of the UNEP Global Partnership on Atmospheric Mercury Transport and Fate Research. UNEP. http://www.mercurywatch.org/userfiles/file/Telmer%20and%20Veiga%202009%20Springer.pdf.

UNECE, 1998. Protocol of Heavy metals, convention on long-range transboundary air pollution. http://www.unece.org/env/lrtap/hm_h1.html.

UNEP, 2013a. Global mercury assessment. Internet: http://www.unep.org/PDF/PressReleases/GlobalMercuryAssessment2013.pdf.

UNEP, 2013b. Minamata convention on mercury. http://www.mercuryconvention.org/Portals/11/documents/Booklets/Minamata%20Convention%20on%20Mercury_booklet_English.pdf.

UNEP, 2013c. Technical background report for the global mercury assessment. Internet: http://www.amap.no/documents/doc/technical-background-report-for-the-global-mercury-assessment-2013/848.

UNEP, 2014. Assessment of the Mercury Content in Coal Fed to Power Plants and Study of Mercury Emissions from the Sector in India. Central Institute of Mining & Fuel Research (CIMFR) UNEP Chemicals Branch, Geneva, Switzerland. http://www.unep.org/chemicalsandwaste/Portals/9/Mercury/REPORT%20FINAL%2019%20March%202014.pdf.

UNFCCC, 2015. United Nations framework convention on climate change: national reports. http://unfccc.int/national_reports/items/1408.php.

USGS, 2015. Commodity statistics and information. Data retrieved in 2015. http://minerals.usgs.gov/minerals/pubs/commodity/.

Wang, F., Wang, S., Zhang, L., Yang, H., Wu, Q., Hao, J., 2014. Mercury enrichment and its effects on atmospheric emissions in cement plants of China. Atmos. Environ. 92, 421–428.

Wang, S.X., Zhang, L., Li, G.H., Wu, Y., Hao, J.M., Pirrone, N., Sprovieri, F., Ancora, M.P., 2010. Mercury emission and speciation of coal-fired power plants in China. Atmos. Chem. Phys. 10, 1183–1192.

Wu, C., Cao, Y., Dong, Z., Cheng, C., Li, H., Pan, W., 2010. Evaluation of mercury speciation and removal through air pollution control devices of a 190 MW boiler. J. Environ. Sci. 22, 277–282.

Wu, Q., Wang, S., Li, G., Liang, S., Lin, C.-J., Wang, Y., Cai, S., Liu, K., Hao, J., 2016. Temporal trend and spatial distribution of speciated atmospheric mercury emissions in China during 1978–2014. ES T (Environ. Sci. Technol.) 50, 13428–13435.

Wu, Q.R., Wang, S.X., Zhang, L., Song, J.X., Yang, H., Meng, Y., 2012. Update of mercury emissions from China's primary zinc, lead and copper smelters, 2000–2010. Atmos. Chem. Phys. 12, 11153–11163.

Wu, Y., Wang, S., Streets, D.G., Hao, J., Chan, M., Jiang, J., 2006. Trends in anthropogenic mercury emissions in China from 1995 to 2003. ES T (Environ. Sci. Technol.) 40, 5312–5318.

Xu, J.-H., Fleiter, T., Fan, Y., Eichhammer, W., 2014. CO2 emissions reduction potential in China's cement industry compared to IEA's Cement Technology Roadmap up to 2050. Appl. Energy 130, 592–602.

Ye, X., Hu, D., Wang, H., Chen, L., Xie, H., Zhang, W., Deng, C., Wang, X., 2015. Atmospheric mercury emissions from China's primary nonferrous metal (Zn, Pb and Cu) smelting during 1949–2010. Atmos. Environ. 103, 331–338.

Yu, L., Yin, L., Xu, Q., Xiong, Y., 2015. Effects of different kinds of coal on the speciation and distribution of mercury in flue gases. J. Energy Inst. 88, 136–142.

Zhang, L., Daukoru, M., Torkamani, S., Wang, S., Hao, J., Biswas, P., 2013. Measurements of mercury speciation and fine particle size distribution on combustion of China coal seams. Fuel 104, 732–738.

Zhang, L., Wang, S., Wang, L., Wu, Y., Duan, L., Wu, Q., Wang, F., Yang, M., Yang, H., Hao, J., Liu, X., 2015. Updated emission inventories for speciated atmospheric mercury from anthropogenic sources in China. ES T (Environ. Sci. Technol.) 49, 3185–3194.

Zhang, X., Siddiqi, Z., Song, X., Mandiwana, K.L., Yousaf, M., Lu, J., 2012a. Atmospheric dry and wet deposition of mercury in Toronto. Atmos. Environ. 50, 60–65.

Zhang, Y., Jacob, D.J., Horowitz, H.M., Chen, L., Amos, H.M., Krabbenhoft, D.P., Slemr, F., St Louis, V.L., Sunderland, E.M., 2016. Observed decrease in atmospheric mercury explained by global decline in anthropogenic emissions. Proc. Natl. Acad. Sci. Unit. States Am. 113 (3), 526–531.

Zhang, Y., Jaeglé, L., van Donkelaar, A., Martin, R.V., Holmes, C.D., Amos, H.M., Wang, Q., Talbot, R., Artz, R., Brooks, S., Luke, W., Holsen, T.M., Felton, D., Miller, E.K., Perry, K.D., Schmeltz, D., Steffen, A., Tordon, R., Weiss-Penzias, P., Zsolway, R., 2012b. Nested-grid simulation of mercury over North America. Atmos. Chem. Phys. 12, 6095–6111.

Zhao, Y., Wang, S., Duan, L., Lei, Y., Cao, P., Hao, J., 2008. Primary air pollutant emissions of coal-fired power plants in China: current status and future prediction. Atmos. Environ. 42.

Zhao, Y., Zhong, H., Zhang, J., Nielsen, C.P., 2015. Evaluating the effects of China's pollution controls on inter-annual trends and uncertainties of atmospheric mercury emissions. Atmos. Chem. Phys. 15, 4317–4337.